Journal of Solid State Chemistry **162,** 122–127 (2001)
doi:10.1006/jssc.2001.9365, available online at http://www.idealibrary.com on IDEAL®

The Real (Incommensurate Interface Modulated) Structure of $Ni_{6\pm x}Se_5$

L. Norén,* G. Van Tendeloo,† and R. L. Withers*,[1]

*Research School of Chemistry, Australian National University, Canberra, ACT 0200, Australia; and †EMAT, University of Antwerp (RUCA), Groenenborgerlaan 171, B-2020 Antwerpen, Belgium

Received May 29, 2001; in revised form August 8, 2001; accepted August 17, 2001

The high-temperature $Ni_{6\pm x}Se_5$ phase has been carefully re-investigated via electron diffraction and TEM imaging. Electron diffraction reveals an (in general) incommensurately modulated, continuously variable (within narrow limits) reciprocal lattice, indirectly confirming the notion of a continuously variable (within narrow limits) $Ni_{6\pm x}Se_5$ solid solution phase. The superspace group symmetry of the incommensurate interface modulated structure is determined and used to predict the allowed conventional three-dimensional space group symmetries when the primary modulation wavevector locks in to $\frac{1}{2}$a*. The mechanism for accommodating nonstoichiometry is suggested to be the introduction into a $2 \times 1 \times 1$ superstructure of variably spaced, non-conservative (100) APB's characterized by the displacement vector $R = [\frac{1}{4}, \frac{1}{2}, 0]$.

1. INTRODUCTION

In the course of a recent investigation of metal-deficient $M_{2-x}X_2$, B8 related solid solution phases in the nickel and cobalt chalcogenide systems (1, 2), our attention was drawn to several high-temperature phases reported in the metal-rich part of the respective phase diagrams (3–13). The role of metal–metal bonding in stabilizing the structures of metal-rich transition metal chalcogenides has long been of fundamental interest. In the case of the metal-deficient $M_{2-x}X_2$ (M = Co, Ni; X = S, Se, Te) B8-type region of the binary phase diagrams, the two d elements behave very similarly and the various phases found are largely isostructural and independent of the metal ion (1, 2). The phase behavior, however, is quite different at the metal-rich end of the respective phase diagrams. In the case of the cobalt chalcogenides, for example, the only metal-rich phase known is Co_9X_8 of the pentlandite structure type (14, 15). Such a phase, however, does not exist for the nickel chalcogenides (3). The latter, by contrast, show several metal-rich phases (some stable at room temperature and some stable only at elevated temperatures) with a higher metal to chalcogenide ratio (3).

The first of these high-temperature phases is found near the nominal composition Ni_6X_5 (X = S, Se). These compounds are only thermodynamically stable over a limited temperature interval (400–570 and 450–670°C for the sulfide and selenide, respectively (8)) and are reported to be isotypic (6). The phase can, however, be stabilized to room temperature either via rapid quenching or appropriate chalcogenide substitution (8, 9). The average structure of the phase has been reported to be orthorhombic *Bmmb* with cell dimensions $a \sim 3.4$, $b \sim 17.1$, and $c \sim 11.9$ Å in the case of the selenide and $a \sim 3.3$, $b \sim 16.4$, and $c \sim 11.3$ Å in the case of the sulfide (9, 10, 12). (The parent reflections corresponding to this average structure unit cell are labeled **G** in what follows).

Density measurements strongly suggest that this average structure unit cell always contains 20 chalcogen atoms whereas the number of Ni atoms is considered to be able to vary within certain limits around 23 to 24 per unit cell, allowing for the small but persistent deviations in composition reported in the literature (3–6, 9–13). Because of the latter reports, some authors have referred to the phase as a continuously variable solid solution phase. The mechanism for such solid solution, however, is still far from clear. Average structure refinements (10, 12) are largely consistent with the idea of a well-defined, essentially fully occupied chalcogen array into some of the various interstices of which are fitted the required number of Ni atoms (see Fig. 1). The coordination of these Ni atoms by the Se atoms ranges from deformed tetrahedral, to square pyramidal, to octahedral (see Fig. 1c). The majority of the Ni atom sites in these average structure refinements were, however, only partially occupied (10, 12) (see Fig. 1c) so that the distribution of occupied and unoccupied Ni sites remained unclear.

The existence of some very short Ni–Ni contact distances (precluding simultaneous local occupancy) in the underlying average structures (see, for example, the circled pairs of Ni atoms in Fig. 1c) not only necessitates partial occupancies for these sites in the underlying average structures but also provides a rationale or justification of the need for

[1] To whom correspondence should be addressed.

0022-4596/01 $35.00

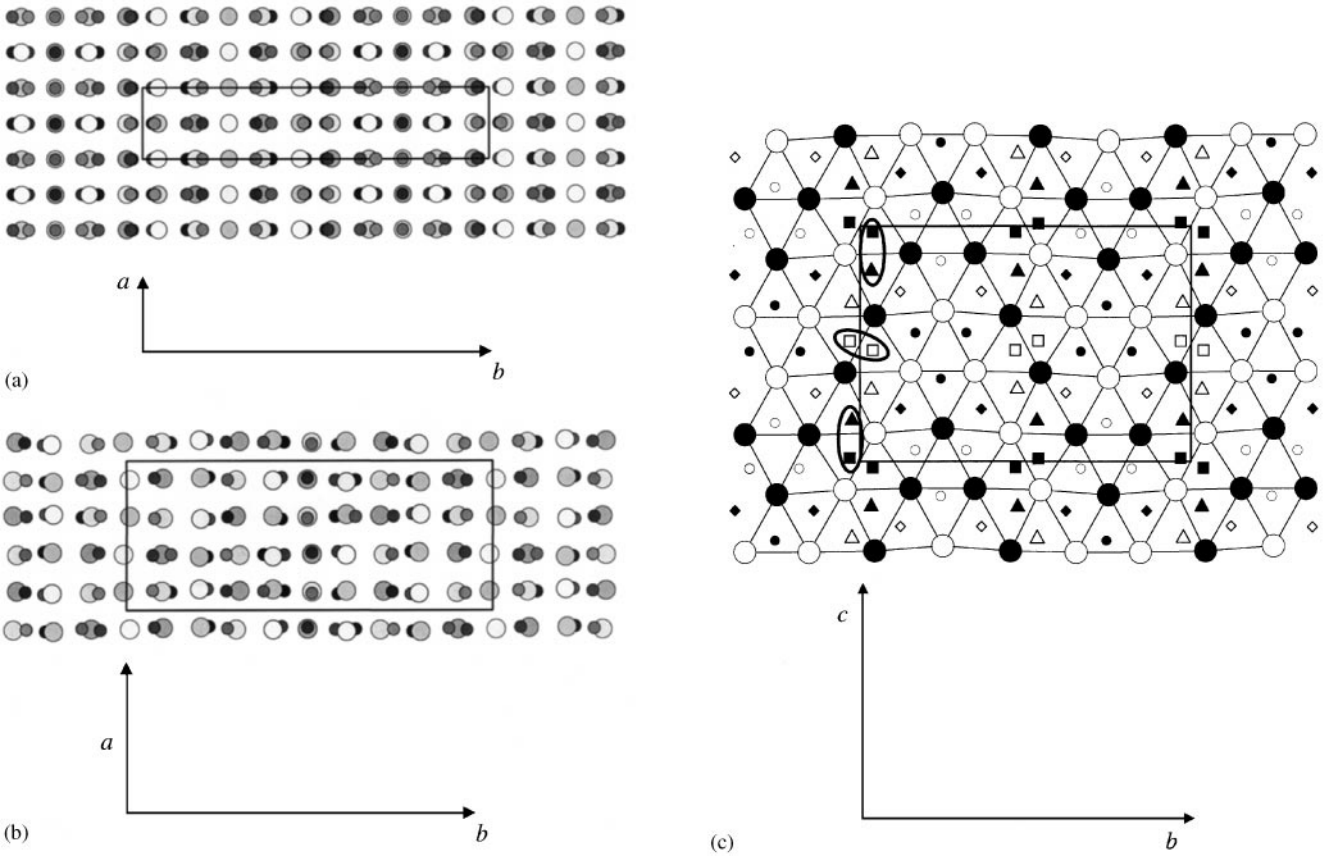

FIG. 1. Shows [001] projections of the reported (a) average crystal structure of Ni_7S_6 (coordinates taken from (12)) and (b) the $2 \times 1 \times 1$ superstructure of Ni_6Se_5 reported by Åkesson and Røst (13). (c) Shows a [100] projection of the average crystal structure of Ni_7S_6. The chalcogen atoms are represented by the larger circles in all cases while the Ni atoms are represented by the smaller symbols (circles in (a) and (b) and circles, squares, triangles, and diamonds in (c)) in all cases. The projected unit cell is outlined in each case. Note the Ni/vacancy ordering and associated structural relaxation (cf. Fig. 1b with Fig. 1a) responsible for the doubled **a** axis in (b). Filled symbols in (c) are at a height of $x = \frac{1}{2}$ while open symbols are at a height of $x = 0$. Circled pairs of Ni atoms represent sites that cannot be simultaneously occupied as a result of the Ni–Ni separation distance being too short. The fully occupied Ni sites in (c) are represented by the circles while the half occupied sites are represented by the square, triangle, and diamond symbols.

additional occupational modulation. Such additional occupational modulation could be expected to give rise to satellite reflections in addition to the strong parent reflections **G** corresponding to the above-average structure unit cells.

Early crystallographic work reported indications of various types of superlattice ordering (giving rise to satellite reflections in addition to the parent reflections **G** corresponding to the above-average structure unit cell) dependent upon the heat treatment used (6, 7, 9–12). This was more recently again mentioned by Åkesson and Røst (13) who reported the crystal structure of Ni_6Se_5 (synthesized by quenching from 420°C) in space group $Pca2_1$ with unit cell parameters $a = 6.863(3)$ Å, $b = 17.09(1)$ Å, and $c = 11.821(5)$ Å, corresponding to a $2 \times 1 \times 1$ superstructure phase. Ni/vacancy ordering and associated structural relaxation (cf., for example, Fig. 1b with Fig. 1a) was shown to be responsible for the observed additional $\mathbf{G} \pm \frac{1}{2}\mathbf{a}^*$ superlattice reflections and, indeed, no partially occupied Ni atom sites remained in the final refined Ni_6Se_5 structure. The question then becomes is the phase truly a line phase of fixed Ni_6Se_5 composition? Or is the composition continuously variable within narrow composition limits? If the latter, what is the mechanism for such compositional flexibility? This paper presents the results of an electron diffraction study of this phase and, indirectly, of its inherent compositional flexibility.

2. EXPERIMENTAL

2.1. Synthesis

Samples of nominal composition Ni_6Se_5 were made by an initial reaction of selenium with nickel cuttings (purity better than 99.99%) at 1000°C for 2–3 h. The reacted material from this procedure was then quenched in water, annealed at 730°C for an additional 4 days followed again by water quenching. The resultant material was then ground, pressed

into pellets, and re-annealed at 570 and 615°C for a week. This procedure was repeated until the X-ray powder patterns, which were taken after each annealing period, remained unchanged. At this point the reaction was assumed to have reached completion. All heat treatments were performed in evacuated silica tubes.

2.2. *X-ray Powder Diffraction*

The average unit cell dimensions of the samples were investigated using a Guinier–Hägg camera. Silicon ($a = 5.4310280$ Å at 22.5°C (16)) was used as an internal standard and the corrected diffraction lines were refined with a least-squares program (17). The resultant average structure cell dimensions were refined to be $a = 3.4347(3)$, $b = 17.0593(12)$, and $c = 11.8547(6)$ Å, in good agreement with previously published results.

3. RESULTS AND DISCUSSION

Figure 2 shows (a) [001], (b) [010], (c) ⟨011⟩ and (d) [100] zone axis electron diffraction patterns (EDPs) typical of this $Ni_{6-x}Se_5$ phase. Integer indexation of the incommensurate EDPs in Fig. 2 is with respect to the four basis vectors $M = \{\mathbf{a}^*, \mathbf{b}^*, \mathbf{c}^*, \mathbf{q} = (\frac{1}{2} + \varepsilon)\mathbf{a}^* - \psi\mathbf{c}^*\}$. (The parameter ε, while small, was often clearly non-zero while the parameter ψ (a non-zero value for which formally lowers the overall symmetry to monoclinic and only pseudo-orthorhombic) is sometimes zero but always very close to zero.) Each individual grain was often found to give a slightly different value for the primary modulation wavevector $\mathbf{q}$, suggesting a continuously variable (within narrow limits) reciprocal lattice. Such behavior is strongly reminiscent of a class of ordered but nonetheless compositionally flexible, incommensurately modulated solid solution phases characterized in reciprocal space by variable incommensurate primary modulation wavevectors directly related to composition (see, for example, (18)). The observation of similar, continuously variable, reciprocal space behavior in the current case indirectly confirms the notion of a continuously variable $Ni_{6-x}Se_5$ solid solution phase and suggests a direct link between reciprocal space behavior and local composition. The implied slight compositional inhomogeneity was not obviously apparent in the Guinier patterns, although it was

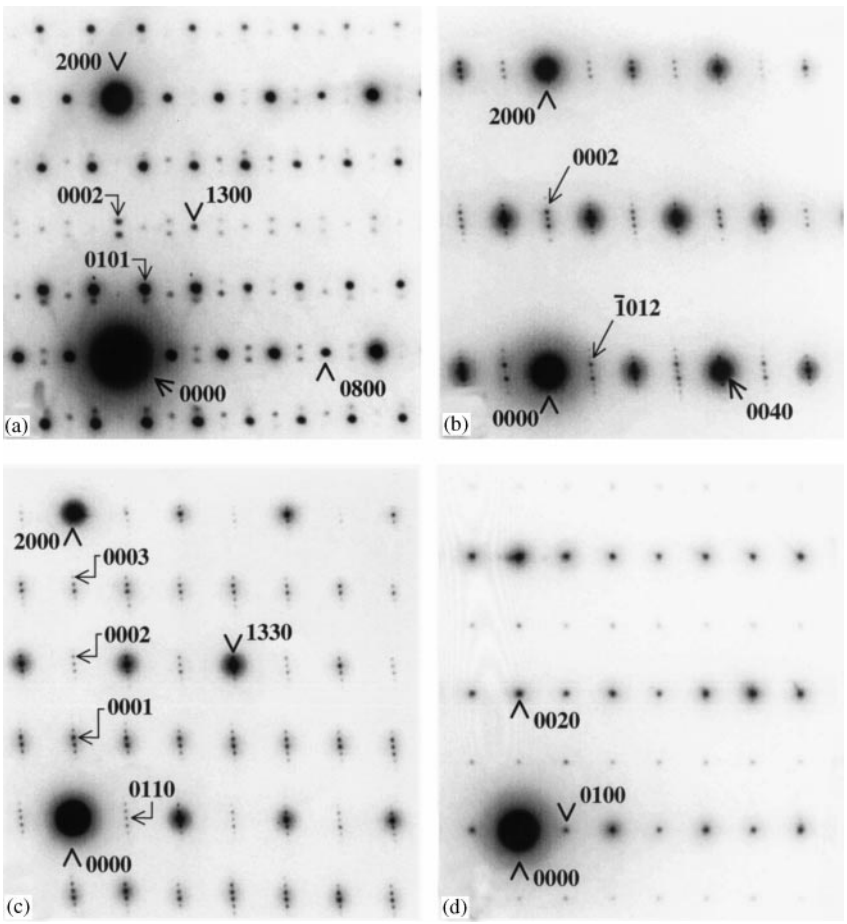

FIG. 2. Shows (a) [001], (b) [010], (c) ⟨011⟩, and (d) [100] zone axis electron diffraction patterns (EDPs) typical of the $Ni_{6-x}Se_5$ solid solution phase. Integer indexation of the incommensurate EDPs in Fig. 2 is with respect to the four basis vectors $M = \{\mathbf{a}^*, \mathbf{b}^*, \mathbf{c}^*, \mathbf{q} = (\frac{1}{2} + \varepsilon)\mathbf{a}^* - \psi\mathbf{c}^*\}$.

certainly true that the longer the specimens were annealed the sharper the corresponding lines became.

In some grains, the primary modulation wavevector **q** had "locked in" to $\frac{1}{2}\mathbf{a}^*$ exactly, giving rise to a reciprocal lattice in agreement (almost) with the structure as proposed by Åkesson and Røst (13) (see Fig. 3a). Figure 3b shows a [001] zone axis EDP, which has also been observed on more than one occasion. In such EDPs a further weak modulation also running along $\mathbf{a}^*$ is apparent. This additional modulation, however, was not always observed and has not been taken into account in what follows.

In general, the EDPs were incommensurate and as shown in Fig. 2. The only observed characteristic extinction conditions are as follows: $F(hk0m) = 0$ unless $h + k + m$ is even (see Fig. 2a) and $F(h0lm) = 0$ unless m is even (see Fig. 2b). The implied superspace group symmetry is at least $P2_1mn(\frac{1}{2}+\varepsilon, 0, 0)1ss$ but most probably $Pmmn(\frac{1}{2}+\varepsilon,\ 0,\ 0)\bar{1}ss$. (Note that we have here ignored the very slight monclinic distortion apparent in Fig. 2b). The corresponding superspace generating operations can be taken to be $\{x_1+\frac{1}{2},\ -x_2,\ -x_3+\frac{1}{2},\ x_4\}$, $\{x_1,\ -x_2+\frac{1}{2},\ x_3,\ x_4+\frac{1}{2}\}$, $\{x_1+\frac{1}{2},\ x_2+\frac{1}{2},\ -x_3+\frac{1}{2},\ x_4+\frac{1}{2}\}$, and $\{-x_1,\ x_2,\ x_3,\ -x_4+2\phi\}$, respectively (18, 19). The resultant conventional space group symmetry if **q** locks in to $\frac{1}{2}\mathbf{a}^*$ is $P12_1/a1$ if the global phase parameter $\phi = (2J+1)/8$, $Pma2$ if $\phi = (2J)/8$, and $P1a1$ otherwise (18–20). Note that the resultant space group symmetry of $Pca2_1$ proposed by Åkesson and Røst (13) for the $2\times1\times1$ superstructure phase of Ni_6Se_5 is not an allowed resultant space group symmetry, given the above superspace group symmetry. This does not necessarily invalidate the refined Ni/vacancy ordering scheme of Åkesson and Røst (13), as shown in Fig. 1b. It does, however, indicate that there is still something significantly wrong with this reported crystal structure despite the apparently reasonable refinement statistics.

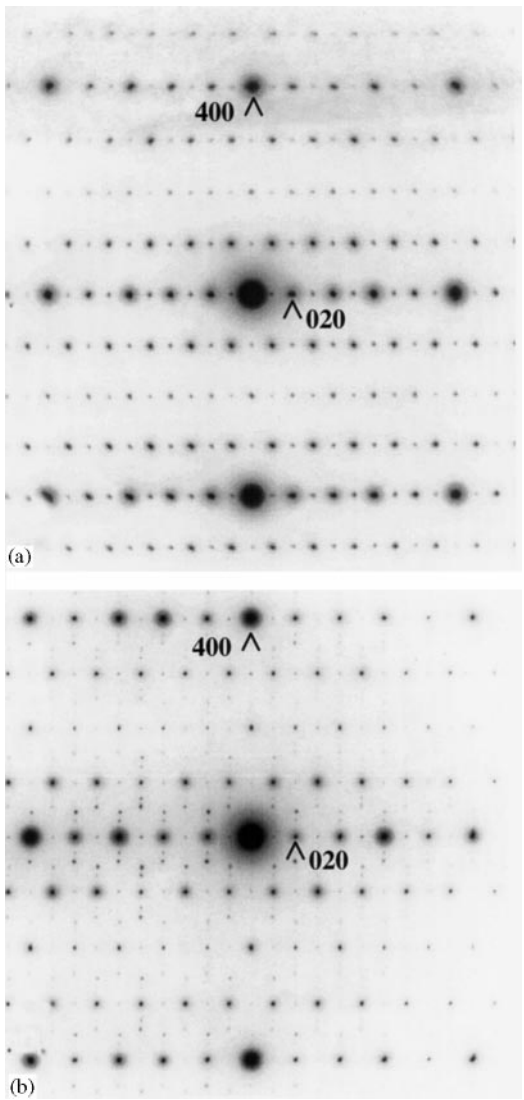

FIG. 3. Shows (a) a [001] zone axis EDP when **q** locks in to $\frac{1}{2}\mathbf{a}^*$ exactly. The indexation is now with respect to the $2\times1\times1$ unit cell given by Åkesson and Røst (13). Figure 3b shows an equivalent [001] zone axis EDP occasionally observed in which a further weak modulation running along $\mathbf{a}^*$ is apparent.

Note that while the underlying average structure has *Pmmn* space group symmetry, it is clearly not too far removed from the commonly assumed *Bmmb* space group symmetry; i.e., the observed reflections that lower the average structure symmetry from *Bmmb* to *Pmmn* are always rather weak as can be seen in Fig. 2. This suggests the need for an additional relatively small amplitude $\mathbf{q} = \mathbf{a}^*$ modulation (presumably primarily compositional, i.e., Ni/vacancy, in origin, although associated displacive relaxation is also only to be expected) to be added to the underlying average structure shown in Fig. 1a. It is interesting to note that *Pmmn* is a subgroup of *Bmmb* and that a condensed modulation transforming according to one particular irreducible representation associated with $\mathbf{q} = \mathbf{a}^*$ is capable of transforming the average structure from *Bmmb* to the required *Pmmn* space group symmetry.

The presence of a multitude of higher order harmonic satellite reflections in Figs. 2a–2c suggests strongly anharmonic/crenel-like atomic modulation functions (AMFs) for the various Ni occupied atomic domains in superspace ultimately required to describe the real space Ni/vacancy distribution (see, for example, (21)). This is perhaps only to be expected given one accepts the previously published structure refinements (see Fig. 1) in conjunction with the notion of a fully Ni/vacancy ordered structure. Refinement of the shape of these Ni occupied atomic domains and the associated displacive relaxations in superspace (particularly in the vicinity of interface regions) would be the ultimate aim of an incommensurate structure refinement if an appropriate single crystal could ever be obtained. (The latter, however, is not likely to be an easy task given the variability from grain to grain, despite the

several week annealing times used, reported in the current contribution.) An alternative to this superspace AMF approach and (to zeroth order) equivalent way of describing the real space Ni/vacancy ordering distribution is to start with the proposed fully ordered $2 \times 1 \times 1$ superstructure phase (see Fig. 1b) and then to introduce appropriately spaced periodic planar translation defects in such a way as to explain the observed reciprocal space incommensurability.

Consider, for example, the [001] zone axis EDP of this superstructure indexed as shown in Fig. 3a. Comparing this EDP with that shown in Fig. 2a, it is apparent that each of the sharp reflections in Fig. 3a have split into a series of satellite reflections along **a*** in Fig. 2a, usually centered about a central satellite reflection whose position has shifted with respect to the corresponding sharp reflection in Fig. 3a. The only unshifted reflections in Fig. 2a correspond to the parent reflections of the underlying average structure as discussed above. On the other hand, $0k0$ reflections with $k = 2J + 1$ in Fig. 2a, for example, are symmetrically shifted, corresponding to a real space periodicity of about 38 Å along a. Such a splitting and shifting of reflections is characteristic of an interface modulated structure characterized by periodic planar translation defects, the separation of the defects being inversely proportional to the splitting of the reflections (22).

The displacement vector **R** (in terms of the $2 \times 1 \times 1$ superstructure unit cell) associated with the translation defect or antiphase boundary (APB) can be determined from the corresponding diffraction patterns by the so-called "fractional shift method" (22). According to this method, the shift of any given reflection of the Ni_6Se_5 superstructure phase (see Fig. 3a) is determined by the dot product $\mathbf{g} \cdot \mathbf{R}$. Knowing the shift of the closest reflection away from its ideal position in Fig. 3a for each **g** allows **R** to be determined. In the present case, these shifts are given by

$$0 \text{ for } \mathbf{g} = 020, \text{ i.e., } 0200 \equiv 020 + \mathbf{0}$$

$$\tfrac{1}{2} \text{ for } \mathbf{g} = 010, \text{ e.g., } \bar{1}102 \equiv 010 + 2\varepsilon\mathbf{a}^*$$

$$\tfrac{1}{2} \text{ for } \mathbf{g} = 200, \text{ e.g., } 0002 \equiv 200 + 2\varepsilon\mathbf{a}^*$$

$$\tfrac{1}{4} \text{ for } \mathbf{g} = 100, \text{ e.g., } 0001 \equiv 100 + \varepsilon\mathbf{a}^*$$

$$0 \text{ for } \mathbf{g} = 001, \text{ i.e., } 0010 \equiv 001 + \mathbf{0}.$$

The corresponding displacement vector (in terms of the superstructure unit cell) is therefore necessarily given by $\mathbf{R} = [\frac{1}{4}, \frac{1}{2}, 0]$.

Real space HREM imaging along [001] confirms this interpretation in terms of APBs. Figure 4, for example, shows (in the thinner regions near the crystal edge) a centered rectangular pattern of dots with a unit mesh size of 6.8×17 Å (i.e., the projected $2 \times 1 \times 1$ superstructure unit cell). The accompanying "stripe" modulation running approximately along (100) is much more apparent in the thicker regions away from the crystal edge. From the contrast within the stripes, it is clear that successive stripes are out of phase by $\frac{1}{2}$ along **b** (see Fig. 4), in agreement with the **b** component of the above deduced displacement vector. The interplanar spacing of these stripes or APBs in Fig. 4 is $\sim$40 Å, in agreement with the distance deduced from the separation between satellite reflections in the corresponding EDP (see Fig. 2a).

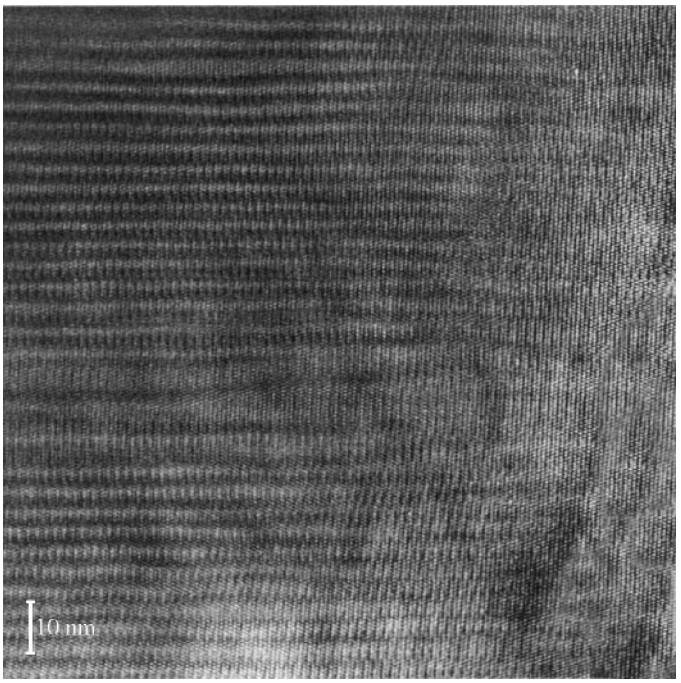

FIG. 4. Shows a real space HREM image taken along [001] (corresponding to the [001] zone axis EDP of Fig. 2a). The **a** axis is again vertical and the **b** axis horizontal. Note the centered rectangular pattern of dots with a unit mesh size of 6.8×17 Å (i.e., the projected $2 \times 1 \times 1$ superstructure unit cell) in the thinner regions near the crystal edge. Note also an accompanying "stripe" modulation running approximately (although not exactly) along (100), which is rather more apparent in the thicker regions away from the crystal edge.

A displacement vector $\mathbf{R} = [\frac{1}{4}, \frac{1}{2}, 0]$ in conjunction with an APB plane of (100) implies that the APB is nonconservative and clearly provides a potential mechanism for varying stoichiometry (see Fig. 1b) while maintaining a fully ordered Ni/vacancy distribution. Careful consideration of Fig. 1b suggests that a regularly spaced sequence of appropriately placed $[\frac{1}{4}, \frac{1}{2}, 0]$ APBs could indeed systematically alter the initial Ni_6Se_5 stoichiometry. Direct confirmation that this is or is not the case, however, must await the results of a rather more detailed and quantitative HREM study of

the Ni ordering both within the $2 \times 1 \times 1$ regions and in the vicinity of the APBs themselves.

4. CONCLUSIONS

It would appear that the $2 \times 1 \times 1$ superstructure refinement of Ni_6Se_5 given by Åkesson and Røst (13; see Fig. 1b) represents a reasonable first approximation to the actual crystal structure of the high-temperature $Ni_{6\pm x}Se_5$ solid solution for $x = 0$, although even for $x = 0$ there is clearly a need for an additional $\mathbf{q} = \mathbf{a}^*$ modulation capable of transforming the average structure from *Bmmb* to the required *Pmmn* space group symmetry. A rather more detailed and quantitative HREM study is needed to understand the crystal chemical origin of this symmetry lowering as well as to confirm the direct correlation between stoichiometry and APB spacing. (Such a study is underway but the results are not immediately evident as a result of the instability of the modulation under an intense electron beam.) The mechanism for accommodating nonstoichiometry for $x \neq 0$ has been suggested to be the introduction of variably spaced, nonconservative (100) APBs characterized by the displacement vector $\mathbf{R} = [\frac{1}{4}, \frac{1}{2}, 0]$.

ACKNOWLEDGMENTS

Reciprocal space investigation was carried out using a Philips EM 430 at the ANU Electron Microscope Unit; real space characterization was performed at the University of Queensland (Centre for Microscopy and Microanalysis, CMM), using a Jeol 4010 electron microscope. The assistance of Dr. John Barry at CMM is gratefully acknowledged as is Ms. Valeska Ting at ANU for help with synthesis.

REFERENCES

1. L. Norén, V. Ting, R. L. Withers, and G. Van Tendeloo, *J. Solid State Chem.*, in press.
2. L. Norén, R. L. Withers, F. J. García-García, and A.-K. Larsson, *Solid State Surf. Sci.*, in press.
3. T. B. Massalski, Ed. "Binary Alloy Phase Diagrams." Am. Soc. Metals, Metals Park, OH, 1986.
4. D. Lundqvist, *Arkiv. Kemi Mineral. Geol. A* **24**(21), (1947).
5. V. G. Kuznecov, A. A Eliseev, Z. S. Spak, K. K. Palkina, M. A. Sokolova, and A. V. Dmitriev, *Voprosy Met. Fiz.* 159 (1961).
6. F. Grønvold, R. Møllerud, and E. Røst, *Acta Chem. Scand.* **20,** 1997 (1966).
7. H. Haraldsen, R. Møllerud, and E. Røst, *Acta Chem. Scand.* **21,** 1727 (1967).
8. A. L. N. Stevels, *Philips Res. Rep., Suppl.* (9), 124 pp (1969).
9. K. Haugsten and E. Røst, *Acta Chem. Scand.* **23,** 3599 (1969).
10. E. Røst and K. Haugsten, *Acta Chem. Scand.* **25,** 3194 (1971).
11. K. L. Komarek and K. Wessely, *Monatsh. Chem.* **103,** 923 (1972).
12. M. E. Fleet, *Acta Crystallogr. B* **28,** 1237 (1972).
13. G. Åkesson and E. Røst, *Acta Chem. Scand. A* **29,** 236 (1975).
14. F. Bøhm, F. Grønvold, H. Haraldsen, and H. Prydz, *Acta Chem Scand.* **9,** 1510 (1955).
15. M. Lindqvist, D. Lundqvist, and A. Westergren, *Svensk. Kem. Tidskr.* **48,** 156 (1936).
16. M. Hart, *J. Crystal Growth* **55,** 409 (1981).
17. Bengt Noläng, Dept. of Materials Chemistry, Ångstrom Laboratory, Uppsala, Sweden.
18. R. L. Withers, S. Schmid, and J. G. Thompson, *Prog. Solid State Chem.* **26,** 1 (1998).
19. S. van Smaalen, *Cryst. Rev.* **4,** 79 (1995).
20. J. M. Pérez-Mato, *in* "Methods of Structural Analysis of Modulated Structures and Quasicrystals" (J. M. Pérez-Mato, F. J. Zúñiga, and G. Madariaga, Eds.), pp. 117–128. World Scientific, 1991.
21. L. Elcoro, J. M. Pérez-Mato, and R. Withers, *Z. Kristallogr.* **215,** 727 (2000).
22. J. Van Landuyt, R. De Ridder, R. Gevers, and S. Amelinckx, *Mater. Res. Bull.* **5,** 353 (1970).